Graphical Abstract

Optimizing irrigation and fertilizer strategy using a crop growth model with delayed nutrient absorption dynamics

Carla J. Becker, Tarek I. Zohdi

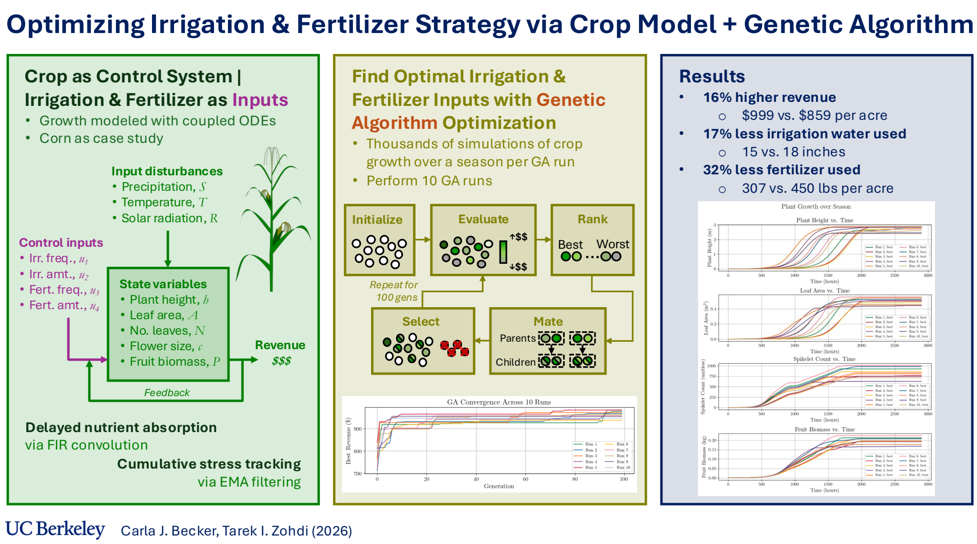

Highlights

Optimizing irrigation and fertilizer strategy using a crop growth model with delayed nutrient absorption dynamics

Carla J. Becker, Tarek I. Zohdi

- Reduced-order coupled ODE model; efficient alternative to DSSAT/APSIM
- FIR convolution formulation for delayed nutrient absorption dynamics
- EMA filtering for cumulative environmental stress tracking
- GA optimization of irrigation/fertilization schedules to maximize revenue
- Calibration and validation against Iowa corn agronomic data

Optimizing irrigation and fertilizer strategy using a crop growth model with delayed nutrient absorption dynamics

Carla J. Becker, Tarek I. Zohdi

[a]*Department of Mechanical Engineering, University of California, Berkeley, 6141 Etcheverry Hall, Berkeley, 94720, California, United States of America*
[b]*Department of Mechanical Engineering, University of California, Berkeley, 6141 Etcheverry Hall, Berkeley, 94720, California, United States of America*

Abstract

Context Rising production costs and declining commodity prices have motivated farmers to seek computational tools for optimizing resource application. While sophisticated crop models such as DSSAT and APSIM simulate detailed physiological processes, they require extensive parameterization and may be computationally expensive for optimization applications. Moreover, existing optimization approaches often use simplified plant response models that do not capture the delayed, cumulative effects of resource application.
Objective This study develops a reduced-order crop growth model that captures delayed nutrient absorption dynamics and couples it with a genetic algorithm to optimize irrigation and fertilizer strategies that maximize net revenue while minimizing input costs.
Methods We present a generalized, coupled ordinary differential equation (ODE) model tracking five state variables—plant height, leaf area, number of leaves, flower size, and fruit biomass—each governed by logistic growth with time-varying growth rates and carrying capacities. These parameters are modulated by nutrient factors quantifying how well actual water, fertilizer, temperature, and solar radiation levels match expected values. Delayed physiological response is captured using finite impulse response (FIR) convolution with Gaussian kernels, where different temporal spreads represent distinct metabolic timescales for each input type. Cumulative stress from sustained deviations is tracked using exponential moving average (EMA) filters. A genetic algorithm searches over application frequency and amount for both irrigation and fertilizer, evaluating candidate strategies through full-season

simulations. The framework is demonstrated using corn grown in Fairfax, Iowa, with historical weather data under a drought scenario (50% of typical precipitation).

Results and Conclusions The genetic algorithm identifies non-intuitive strategies that outperform conventional uniform application schedules, achieving 16% higher net revenue ($999 vs. $859 per acre) through strategic timing of resource inputs. The optimized strategies use 17% less irrigation (15 vs. 18 inches) and 32% less fertilizer (307 vs. 450 lbs) than farmer best practices while achieving comparable or higher crop yields. Across 10 independent optimization runs, 9 outperformed the baseline, demonstrating algorithm robustness.

Significance These results demonstrate that under delayed absorption dynamics, timing of inputs matters more than total quantity—a finding that challenges conventional drought response strategies of increased irrigation frequency. The framework offers a computationally tractable alternative to complex mechanistic models for precision agriculture optimization and is generalizable to other crops through re-parameterization.

Keywords: precision agriculture, resource optimization, crop growth model, genetic algorithm, cumulative stress tracking

---

1. Introduction

The agriculture sector in the United States faces significant challenges as the number of farms declines and the cost of farming continues to rise [1]. Rising production expenses for equipment, seeds, and labor, coupled with elevated interest rates and declining commodity prices, have made farming increasingly expensive. To navigate this challenging landscape, farmers are employing strategies such as cost management and operational optimization. One promising approach is to use modeling and simulation to optimize farm operations without substantial capital investment. Recent advances in computational methods have enabled sophisticated digital-twin frameworks for precision agriculture [2, 3], and machine learning techniques have been applied to optimize sensor placement and resource delivery in agricultural systems [4, 5].

Mathematical modeling of crop growth has a rich history, with models ranging from simple empirical relationships to complex mechanistic simulations. Logistic growth models, first proposed by Verhulst in 1838, remain widely used due to their interpretability and ability to capture resource-limited growth dynamics [6]. More sophisticated crop models such as DSSAT [7], APSIM [8], and WOFOST [9] simulate detailed physiological processes but require extensive parameterization and may be computationally expensive for optimization applications. In contrast, reduced-order models that capture essential dynamics while remaining tractable for optimization have gained attention in precision agriculture [10].

Optimization of irrigation and fertilizer application has been studied using various approaches, including linear and nonlinear programming [11], dynamic programming [12], and metaheuristic algorithms [13]. Genetic algorithms (GAs) are particularly well-suited for this domain because they can handle nonlinear, non-convex objective functions and do not require gradient information [14]. Previous work has applied GAs to irrigation scheduling [15] and fertilizer optimization [16], but these studies often use simplified plant response models that do not capture the delayed, cumulative effects of resource application.

This paper presents a generalized, coupled ordinary differential equation (ODE) model for crop growth that addresses these limitations. The model captures: (1) nonlinear logistic growth with state-dependent carrying capacities, (2) delayed absorption of water, fertilizer, temperature, and solar radiation inputs through finite impulse response (FIR) convolution, (3) cumulative stress tracking via exponential moving average (EMA) filters, and (4) coupling between vegetative and reproductive growth stages. The model is designed to enable global optimization under delayed, resource-coupled dynamics—a regime where even well-established management practices may benefit from computational refinement due to the sheer number of possible scheduling combinations.

We demonstrate the framework by optimizing irrigation and fertilizer strategies for corn, the most widely planted crop in the United States by acreage. Using a genetic algorithm, we search for strategies that maximize net revenue (crop value minus input costs) over a growing season. The approach is validated using historical weather data from Fairfax, Iowa, a representative location in the Corn Belt.

2. Generalized, coupled-ODE crop model

The proposed model tracks five state variables representing key aspects of plant development: plant height h (m), leaf area per leaf A (m^2), number of leaves N, flower size c (number of spikelets), and fruit biomass P (kg). Each state variable follows logistic growth dynamics with time-varying growth rates and carrying capacities that depend on environmental conditions and resource availability.

The model receives four input signals: water from irrigation w (inches), fertilizer application f (lbs), ambient temperature T (°C), and solar radiation R (W/m^2). Precipitation S (inches) is added to irrigation to obtain total water input. Temperature and radiation data are obtained from the National Solar Radiation Database (NSRDB) [17], while precipitation data comes from NOAA historical records [18].

2.1. Delayed absorption via FIR convolution

Plants do not immediately process applied nutrients; instead, there is a physiologically-mediated delay between application and utilization. We model this delayed absorption using finite impulse response (FIR) convolution with Gaussian kernels.

If cumulative nutrient uptake follows a sigmoid trajectory—with slow initial uptake due to transport lag, rapid increase once metabolic pathways activate, and eventual saturation—then instantaneous absorption rate follows a bell-shaped curve. A Gaussian kernel is the least assumptive choice for a bell curve, requiring only two parameters: the temporal spread σ (characterizing absorption duration) and the peak delay μ.

Given only the temporal spread σ for each nutrient type, we determine μ such that 95% of the kernel mass lies within $[0, 2\mu]$. This requires solving

$$\operatorname{erf}\left(\frac{\mu}{\sigma\sqrt{2}}\right) = 0.95, \tag{1}$$

which yields $\mu \approx 1.96\sigma$. The Gaussian FIR kernel is then

$$g[k] = \frac{1}{\sqrt{2\pi\sigma^2}} \exp\left\{-\frac{1}{2}\frac{(k-\mu)^2}{\sigma^2}\right\}. \tag{2}$$

The FIR horizon L^* is chosen as the minimum length capturing 95% of the kernel mass:

$$L^* = \min_L \left\{ L : \frac{\sum_{k=0}^{L-1} g[k]}{\sum_{k=0}^{K-1} g[k]} \geq 0.95 \right\} \tag{3}$$

where K is the simulation length in hours.

Different nutrients have different metabolic timescales. We use $\sigma_w = 30$ hours for water (rapid uptake), $\sigma_f = 300$ hours for fertilizer (slow uptake reflecting root absorption dynamics), and $\sigma_T = \sigma_R = 30$ hours for temperature and radiation (immediate physiological effects with short memory).

2.2. Cumulative stress tracking via EMA filtering

While FIR convolution captures delayed absorption, plants also accumulate stress from sustained deviations from optimal conditions. We model this cumulative effect using exponential moving average (EMA) filters, which are equivalent to first-order infinite impulse response (IIR) systems.

The EMA filter with memory parameter $\beta \in [0, 1)$ has the recursive form:

$$y[k] = (1 - \beta)x[k] + \beta y[k-1] \tag{4}$$

where larger β values correspond to longer memory (slower response to changes). This formulation preserves constant signals ($x[k] = c$ implies $y[k] \to c$) while smoothing transient fluctuations.

2.3. Nutrient factor calculation

We now describe the complete transformation pipeline that converts raw input signals into nutrient factors $\nu \in [0, 1]$ that modulate plant growth. Using fertilizer as an example (the same process applies to water, temperature, and radiation):

Step 1: Delayed absorption. Convolve the raw fertilizer signal $f[k]$ with the Gaussian FIR kernel:

$$\bar{f}[k] = \sum_{n=0}^{L_f - 1} g_f[n] f[k-n] \tag{5}$$

Step 2: Cumulative absorption. Compute the running sum of absorbed fertilizer:

$$F[k] = \sum_{n=0}^{k} \bar{f}[n] \tag{6}$$

Step 3: Instantaneous anomaly. Compare actual cumulative absorption to expected levels:

$$\delta_f[k] = \left| \frac{k \cdot f_{\text{typ}} - F[k]}{k \cdot f_{\text{typ}} + \epsilon} \right| \tag{7}$$

where f_{typ} is the typical hourly fertilizer level the plant "expects" and ϵ is a small constant preventing division by zero.

Step 4: Cumulative divergence. Apply EMA smoothing to track sustained anomalies:

$$\Delta_f[k] = \beta_\Delta \Delta_f[k-1] + (1-\beta_\Delta)\delta_f[k] \tag{8}$$

where $\beta_\Delta = 0.95$ provides long memory.

Step 5: Nutrient factor. Convert divergence to a stress factor via exponential decay with additional EMA smoothing:

$$\nu_f[k] = \beta_\nu \nu_f[k-1] + (1-\beta_\nu)\exp\{-\alpha\Delta_f[k]\} \tag{9}$$

where $\alpha = 3$ ensures $\nu \approx 0.05$ when $\Delta = 1$ (complete divergence from expected levels), and $\beta_\nu = 0.05$.

The nutrient factor $\nu_f[k]$ equals 1 when fertilizer application perfectly matches expected levels and decays toward 0 under sustained over- or under-application. This captures the intuition that plants are resilient to brief deviations but suffer cumulative damage from prolonged stress.

Figure 1 illustrates the FIR convolution and EMA smoothing operations that constitute the metabolic transformation pipeline. The left panel shows how the Gaussian FIR kernel spreads and delays input signals, while the right panel demonstrates how EMA filtering with different β values tracks cumulative divergence with varying memory lengths.

2.4. Effects of inputs on plant growth

Different inputs affect different aspects of plant growth. Tables 1 and 2 summarize these relationships based on agronomic literature [19, 20, 21].

State variable	Irrigation on growth rate	Fertilizer on growth rate	Irrigation on capacity	Fertilizer on capacity
Plant height h	$\sim$	$+$	$\sim$	$+$
Leaf area A	$\sim$	$+$	$+$	$+$
Number of leaves N	$\sim$	$\sim$	$\sim$	$\sim$
Flower size c	$\sim$	$\sim$	$+$	$\sim$
Fruit biomass P	$\sim$	$\sim$	$+$	$+$

Table 1: Effects of irrigation and fertilizer on growth dynamics. "+" indicates positive effect, "$\sim$" indicates a negligible effect.

State variable	Temp. on growth rate	Temp. on capacity	Radiation on growth rate	Radiation on capacity
Plant height h	$+$	$+$	$+$	$+$
Leaf area A	$+$	$+$	$+$	$+$
Number of leaves N	$\sim$	$+$	$\sim$	$+$
Flower size c	$-$	$-$	$-$	$-$
Fruit biomass P	$+$	$+$	$+$	$+$

Table 2: Effects of temperature and solar radiation on growth dynamics. "+" indicates positive effect, "$\sim$" indicates a negligible effect, "–" indicates a negative effect. For flower size, excess heat and radiation reduce flower development, hence negative effects.

2.5. Growth dynamics

Each state variable follows logistic growth with time-varying parameters modulated by nutrient factors. The general form is:

$$\frac{dx}{dt} = \hat{a}_x(t) \cdot x(t) \left(1 - \frac{x(t)}{\hat{k}_x(t)}\right) \tag{10}$$

where $\hat{a}_x(t)$ is the effective growth rate and $\hat{k}_x(t)$ is the effective carrying capacity, both functions of the nutrient factors.

The effective parameters are computed as geometric means of the relevant nutrient factors, reflecting multiplicative rather than additive effects. This choice is motivated by the observation that growth rates compound over time, making geometric averaging appropriate [22].

Plant height responds to fertilizer, temperature, and radiation:

$$\hat{a}_h(t) = a_h(\nu_f \nu_T \nu_R)^{1/3}, \quad \hat{k}_h(t) = k_h(\nu_f \nu_T \nu_R)^{1/3} \tag{11}$$

Leaf area additionally depends on water and is coupled to height:

$$\hat{a}_A(t) = a_A(\nu_f \nu_T \nu_R)^{1/3}, \quad \hat{k}_A(t) = k_A \left(\nu_w \nu_f \nu_T \nu_R \frac{\hat{k}_h}{k_h} \right)^{1/5} \tag{12}$$

Number of leaves depends only on temperature and radiation through the carrying capacity:

$$\hat{a}_N(t) = a_N, \quad \hat{k}_N(t) = k_N(\nu_T \nu_R)^{1/2} \tag{13}$$

Flower size (spikelet count) exhibits inverse dependence on temperature and radiation—excess heat and light reduce flowering:

$$\hat{a}_c(t) = a_c \left(\frac{1}{\nu_T} \frac{1}{\nu_R} \right)^{1/2}, \quad \hat{k}_c(t) = k_c \left(\nu_w \frac{1}{\nu_T} \frac{1}{\nu_R} \right)^{1/3} \tag{14}$$

Fruit biomass depends on all inputs and is coupled to vegetative growth:

$$\hat{a}_P(t) = a_P \left(\frac{1}{\nu_T} \frac{1}{\nu_R} \right)^{1/2}, \quad \hat{k}_P(t) = k_P \left(\nu_w \nu_f \nu_T \nu_R \frac{\hat{k}_h}{k_h} \frac{\hat{k}_A}{k_A} \frac{\hat{k}_c}{k_c} \right)^{1/7} \tag{15}$$

The coupling terms $\hat{k}_h/k_h$, $\hat{k}_A/k_A$, and $\hat{k}_c/k_c$ encode physiological dependencies: taller plants with more leaf area can support larger fruit, while larger tassels (more spikelets) may compete with ear development.

2.6. Model parameters

The baseline growth rates and carrying capacities are crop-specific parameters that can be estimated from field data or literature values. For corn, we use the values in Table 3, calibrated to match typical development timelines where plants reach full vegetative size around 65–70 days after sowing and grain fill completes around 125 days [23].

State	Growth rate	Carrying capacity	Initial condition	Units
Height h	$a_h = 0.010$ hr^{-1}	$k_h = 3.0$	$h_0 = 0.001$	m
Leaf area A	$a_A = 0.0105$ hr^{-1}	$k_A = 0.65$	$A_0 = 0.001$	m^2
Leaves N	$a_N = 0.011$ hr^{-1}	$k_N = 20$	$N_0 = 0.001$	count
Spikelets c	$a_c = 0.010$ hr^{-1}	$k_c = 1000$	$c_0 = 0.001$	count
Fruit P	$a_P = 0.005$ hr^{-1}	$k_P = 0.25$	$P_0 = 0.001$	kg

Table 3: Baseline model parameters for corn. Growth rates are per hour; initial conditions are set to k_x/K where $K \approx 2900$ is the season length in hours.

3. Simulation

The logistic ODE admits a closed-form solution, enabling exact time-stepping without numerical integration error. Given state $x(t)$ at time t, the state at $t + \Delta t$ is:

$$x(t+\Delta t) = \frac{\hat{k}_x(t)}{1 + \left(\dfrac{\hat{k}_x(t)}{x(t)} - 1\right)\exp(-\hat{a}_x(t)\Delta t)} \tag{16}$$

where $\hat{a}_x(t)$ and $\hat{k}_x(t)$ are treated as constant over the time step. This closed-form approach is more accurate than forward Euler integration and avoids instability issues that can arise with explicit methods at larger time steps.

We simulate the growing season at hourly resolution ($\Delta t = 1$ hour), yielding approximately 2900 time steps for a typical corn season (late April to early October). At each step, we: (1) update the nutrient factors based on cumulative inputs and divergences, (2) compute effective growth rates and carrying capacities, and (3) advance each state variable using Equation 16.

4. Optimization via genetic algorithm

Given the nonlinear, delay-affected dynamics of the crop model, gradient-based optimization is challenging. The delayed effects of inputs create a non-convex landscape with potentially many local optima. We therefore employ a genetic algorithm (GA), a population-based metaheuristic inspired by natural selection that can effectively explore complex search spaces [14].

4.1. Decision variables

Each candidate solution encodes a complete irrigation and fertilization strategy as a four-dimensional vector:

$$\mathbf{u} = \begin{bmatrix} u_1 \\ u_2 \\ u_3 \\ u_4 \end{bmatrix} = \begin{bmatrix} \text{irrigation frequency (hours)} \\ \text{irrigation amount (inches)} \\ \text{fertilizer frequency (hours)} \\ \text{fertilizer amount (lbs)} \end{bmatrix} \tag{17}$$

The frequencies specify application intervals: $u_1 = 168$ means irrigate every 168 hours (weekly). The amounts specify the quantity applied at each event. This parameterization assumes regular, periodic application—a simplification that captures common agricultural practice while keeping the search space tractable.

4.2. Objective function

The objective is to maximize net revenue, defined as crop value minus input costs.

$$\text{Revenue}(\mathbf{u}) = \text{Crop Value} - \text{Input Costs} \tag{18}$$

The crop value depends on final plant state at harvest:

$$\text{Crop Value} = \omega_h h[K] + \omega_A A[K] + \omega_P P[K] \tag{19}$$

where K is the final time step and ω_h, ω_A, ω_P are economic weights (dollars per unit) for height, leaf area, and fruit biomass respectively.

The input costs accumulate over the season:

$$\text{Input Costs} = \omega_w \sum_{k=0}^{K} w[k] + \omega_f \sum_{k=0}^{K} f[k] \tag{20}$$

where ω_w and ω_f are costs per unit of irrigation and fertilizer.

For corn, the economic weights are derived from market prices and typical yields (Table 4). The fruit biomass weight dominates, reflecting that grain yield is the primary economic output.

Parameter	Value	Derivation
ω_w	\$2.00/inch	Typical irrigation cost
ω_f	\$0.61/lb	Weighted NPK cost
ω_h	\$35/m	Silage value proxy
ω_A	\$215/m^2	Silage value proxy
ω_P	\$4,450/kg	\$4/bushel $\times$ plant density

Table 4: Economic weights for the corn objective function. The fruit biomass weight accounts for approximately 28,350 plants per acre at \$0.157/kg.

4.3. Algorithm description

The GA maintains a population of M candidate solutions and iteratively improves them through selection, crossover, and mutation over G generations. Algorithm 1 presents the complete procedure.

Selection. After each generation, population members are ranked by cost. The top P members survive as "parents" for the next generation. This selection ensures the best solutions are never lost.

Crossover. New "children" are created by blending two parent solutions. For each child, we randomly select two parents and compute a weighted average:

$$\mathbf{u}^{(\text{child})} = \phi \cdot \mathbf{u}^{(a)} + (1 - \phi) \cdot \mathbf{u}^{(b)} \tag{21}$$

where $\phi \sim \text{Uniform}(0, 1)$ under normal operation. This crossover can produce children anywhere along the line segment connecting the parents, enabling smooth exploration of the search space.

Mutation and Diversity. To maintain population diversity and escape local optima, the remaining $M - P - C$ population slots are filled with randomly generated solutions. Additionally, if the best cost stagnates (changes by less than 0.01) for 10 consecutive generations, we switch to aggressive crossover with $\phi \sim \text{Uniform}(-1, 2)$. This allows children to lie outside the convex hull of their parents, promoting exploration of new regions.

Default Parameters. We use $M = 128$ members, $P = 16$ parents, $C = 16$ children, and $G = 100$ generations. The large population relative to generations ensures diversity for exploration while preventing premature convergence.

5. Case study: corn in iowa

We demonstrate the framework using corn, the most widely planted crop in the United States with over 90 million acres harvested annually [24]. The case study uses historical weather data from Fairfax, Iowa (41.76°N, 91.87°W), a representative location in the Corn Belt (USDA climate zones 4b–5b).

5.1. Scenario configuration

The simulation covers a typical growing season from late April to early October (approximately 2900 hours). Environmental inputs are:

- **Temperature and radiation:** Hourly data from NSRDB for Fairfax, IA. Mean temperature is 22.8°C; mean solar radiation is 580 W/m^2.
- **Precipitation:** Daily data from NOAA, interpolated to hourly resolution.
- **Typical nutrient expectations:** Based on agronomic recommendations [25], the model expects 28 inches of water and 355 lbs of NPK fertilizer over the season ($w_{\text{typ}} \approx 0.01$ in/hr, $f_{\text{typ}} \approx 0.12$ lb/hr).

Table 5 summarizes expected corn development timelines used to calibrate model parameters.

State variable	Days to maturity	Hours to maturity	Typical final value
Plant height h	65–70	1560–1680	2.7–3.7 m
Leaf area A	55–65	1320–1560	0.6–0.7 m^2
Number of leaves N	65	1560	18–20
Spikelets c	65–70	1560–1680	$\sim$1000
Fruit biomass P	125	3000	0.15–0.36 kg

Table 5: Corn development timeline and typical final values from agronomic literature [23, 26].

5.2. Baseline scenario: farmer best practices under drought

To establish a performance baseline, we first simulate crop growth under a drought scenario (50% of typical precipitation) using conventional farmer practices: weekly irrigation of 1 inch [27] and monthly fertilizer applications of 90 lbs [28]. These values reflect standard agronomic recommendations for corn in the Corn Belt region.

Figure 2 shows the environmental disturbances and control inputs over the growing season. The reduced precipitation characteristic of a drought year is clearly visible, along with the periodic irrigation and fertilizer applications.

Figure 3 shows the resulting plant state trajectories. Under drought conditions with conventional management, the plant reaches the following final values: height of 2.6 m (vs. 3.0 m capacity), leaf area of 0.57 m^2 (vs. 0.65 m^2), and fruit biomass of 0.22 kg (vs. 0.25 kg). The net revenue under this baseline scenario is \$859/acre.

The baseline scenario demonstrates how the model captures stress effects: despite regular irrigation, the mismatch between applied water and the plant's metabolic expectations under drought conditions leads to sustained nutrient factor depression and reduced growth potential. Detailed visualizations of the applied vs. absorbed nutrients, cumulative values, and nutrient factors are provided in the Supplementary Information.

5.3. Optimization configuration

The GA searches over the following bounds:

- Irrigation frequency: 100–700 hours (4–29 days between applications)
- Irrigation amount: 0.5–5.0 inches per application
- Fertilizer frequency: 700–2900 hours (29–121 days, i.e., 1–4 applications per season)
- Fertilizer amount: 100–500 lbs per application

These bounds reflect practical constraints: irrigation systems have minimum application rates, and fertilizer is typically applied in a small number of large doses rather than continuously. The optimization was performed under the same environmental conditions: a drought scenario with 50% of typical precipitation.

5.4. Optimization results

To assess robustness of the optimization, we executed 10 independent GA runs with different random seeds. Figure 4 shows the convergence of all 10 runs, with each curve representing the best revenue achieved at each generation. All runs converge to similar final values (within 3% of each other), demonstrating that the GA reliably finds near-optimal solutions despite the stochastic nature of the search.

The optimal strategy identified by the GA is summarized in Table 6. Notably, the algorithm discovers a strategy with less frequent but larger irrigation events and infrequent fertilizer applications—a pattern that minimizes cumulative divergence from expected nutrient levels given the model's delayed absorption dynamics.

Parameter	Optimal Value	Interpretation
Irrigation frequency	1237 hours	Every ∼7 weeks
Irrigation amount	5 inches	Per application
Fertilizer frequency	803 hours	Every 33 days
Fertilizer amount	77 lbs	Per application

Table 6: Optimal irrigation and fertilization strategy identified by the GA.

Figure 5 shows the plant state trajectories for the best member in each of the 10 GA runs. All optimized strategies achieve substantially higher final values than the baseline farmer practices: fruit biomass ranges from 0.168–0.225 kg (vs. 0.22 kg baseline), heights reach 2.41–2.88 m (vs. 2.6 m), leaf areas reach 0.44–0.56 m^2 (vs. 0.57 m^2), and revenues reach 778–999 \$/acre (vs. \$859/acre baseline). The consistency across runs further confirms the robustness of the optimization, and while the farmer best practice yields higher revenue than one GA run (run 2), in aggregate, the GA optimization meaningfully improved upon the baseline.

Table 7 provides an economic comparison between the baseline farmer practices and the GA-optimized strategies. The best GA strategy achieves \$999/acre net revenue compared to \$859/acre for the baseline—a 16% improvement. Even the worst members in each GA run's final population outperform the baseline, providing a sanity check that random strategies are not viable (see Supplementary Information).

Metric	GA-Optimized	Baseline
Final fruit biomass	0.22 kg	0.22 kg
Final height	2.8 m	2.6 m
Final leaf area	0.60 m^2	0.57 m^2
Total irrigation	15 inches	18 inches
Total fertilizer	307 lbs	450 lbs
Crop value	\$1218	\$1171
Input costs	\$219	\$312
Revenue	**\$999**	**\$859**

Table 7: Economic comparison of GA-optimized versus baseline farmer strategies. The optimized strategy achieves 16% higher net revenue through both increased crop value and dramatically reduced irrigation costs.

6. Discussion

6.1. Interpretation of results

The GA-optimized strategy differs from conventional wisdom in several notable ways. The algorithm discovers that less frequent but larger irrigation events, combined with reduced total fertilizer input, can outperform conventional uniform application schedules. This counterintuitive result emerges from the model's delayed absorption dynamics: under drought conditions, the plant's metabolic expectations are calibrated to typical water availability. The GA discovers that strategically-timed resource inputs better maintain alignment with metabolic expectations than aggressive compensation for drought through frequent, uniform applications.

The consistency across 10 independent GA runs provides confidence that the optimization reliably identifies high-performing regions of the strategy space. While individual runs converge to somewhat different local optima (with revenues ranging from \$778 to \$983 per acre), 9 of 10 runs outperform the baseline farmer practices, demonstrating the robustness of the optimization approach. The sanity check showing that even the worst members in each final population generally outperform baseline practices confirms that the GA successfully eliminates poor candidates.

The 16% revenue improvement ($999 vs. $859 per acre) demonstrates substantial potential value from model-based optimization. This improvement comes from two sources: (1) increased crop value due to better-aligned nutrient delivery, and (2) reduced input costs. The result suggests that conventional wisdom about drought response—applying more water to compensate—may be suboptimal when plant physiology involves delayed, cumulative-effect dynamics.

6.2. Parameter estimation in practice

The framework requires crop-specific parameters: growth rates, carrying capacities, metabolic timescales, and typical nutrient expectations. Several approaches could estimate these from data:

- **Growth curves:** Time-series imagery from field cameras or drones, processed with computer vision, could provide height and leaf area trajectories for fitting a_x and k_x parameters.
- **Metabolic timescales:** The temporal spreads σ could be estimated from controlled experiments varying input timing, or inferred from physiological literature on nutrient uptake rates.
- **Typical expectations:** Regional agronomic recommendations provide baseline values for w_{typ}, f_{typ}, T_{typ}, and R_{typ}.

Physics-informed neural networks (PINNs) could jointly fit model parameters and approximate unknown functional forms in the dynamics, potentially relaxing some of the structural assumptions in Section 2.

6.3. Limitations and extensions

Several model limitations suggest directions for future work:

Growth model. The logistic equation assumes symmetric growth around the inflection point. Richards growth [29] generalizes this with a shape parameter ν:

$$\frac{dx}{dt} = a_x x \left[1 - \left(\frac{x}{k_x}\right)^{\nu}\right] \tag{22}$$

where $\nu > 1$ produces steeper early growth (common in vegetative stages) and $\nu < 1$ produces steeper late growth.

Absorption kernels. Gaussian kernels are symmetric, but physiological absorption often exhibits fast activation followed by slow decay. Log-normal or Gamma kernels could better capture this asymmetry.

Saturation. The current model does not explicitly limit nutrient uptake—all applied inputs eventually affect the plant. In reality, excess application may be lost to runoff or leaching. Saturating nonlinearities in the absorption pathway would provide a more realistic response to over-application.

Spatial heterogeneity. The model treats a single representative plant. Field-scale optimization would need to account for spatial variation in soil properties, microclimate, and plant density.

Stochastic weather. The case study uses historical weather data. Robust optimization under weather uncertainty, or adaptive strategies that respond to observed conditions, could improve real-world performance.

7. Conclusion

This paper presented a coupled ODE model for crop growth that captures delayed nutrient absorption via FIR convolution and cumulative stress effects via EMA filtering. The model's time-varying growth rates and carrying capacities encode the intuition that plant development depends not just on current conditions but on the history of resource availability relative to physiological expectations.

Applied to corn optimization in Iowa under drought conditions, a genetic algorithm discovered irrigation and fertilizer strategies that achieve 16% higher net revenue than conventional farmer practices ($999 vs. $859 per acre). This improvement emerges from the model's delayed absorption dynamics: strategic timing of inputs that aligns with metabolic expectations outperforms uniform application schedules. The consistency across 10 independent optimization runs, with 9 of 10 outperforming the baseline, confirms the robustness of these findings.

The framework is generalizable to other crops through re-parameterization and offers a computationally tractable approach to input optimization. Future work will extend the model to handle weather uncertainty, incorporate spatial heterogeneity, and validate predictions against field trial data.

8. Supplementary information

This supplementary section provides additional visualizations of the baseline scenario (farmer best practices under drought) and the GA optimization results.

S1. Detailed baseline scenario analysis

Figure 6 shows the applied versus absorbed nutrients under the baseline scenario. The delayed absorption via FIR convolution is clearly visible: the absorbed signals (smoothed curves) lag behind the applied inputs and exhibit the characteristic spreading effect of the Gaussian kernels.

Figure 7 shows the cumulative absorbed nutrients compared to expected (typical) levels. Under drought conditions, actual water absorption falls progressively below expectations, while fertilizer, temperature, and radiation track more closely to typical values.

Figure 8 shows the instantaneous divergence from expected cumulative levels. These divergences, after EMA smoothing, determine the nutrient factors that modulate plant growth.

Figure 9 shows the resulting nutrient factors. The water factor ν_w declines throughout the season as drought stress accumulates, reaching approximately 0.6 by harvest. This reduced water factor is the primary driver of the suboptimal crop growth observed in the baseline scenario.

S2. GA optimization: worst-case analysis

As a sanity check, Figure 10 shows the plant state trajectories for the *worst* member in each GA run's final population. Even these suboptimal strategies—the least fit survivors after 100 generations of evolution—outperform the baseline farmer practices. This confirms that: (1) the GA successfully eliminates poor strategies, and (2) random or arbitrary irrigation/fertilization schedules cannot match even the worst optimized approaches.

9. Acknowledgements

This work has been partially supported by the UC Berkeley College of Engineering and the USDA AI Institute for Next Generation Food Systems (AIFS), USDA award number 2020-67021-32855.

Declarations

Competing Interests The authors declare that they have no known competing financial interests or personal relationships that could have appeared to influence the work reported in this paper.

Code availability The source code used for this study is archived on Zenodo at `https://doi.org/10.5281/zenodo.18204023`.

Declaration of generative AI and AI-assisted technologies in the manuscript preparation process During the preparation of this work the authors used ChatGPT and Claude Code in order to generate some portions of the code base, though no underlying theory, and refine the original drafts of the paper. After using this tool/service, the authors reviewed and edited the content as needed and take full responsibility for the content of the published article.

References

[1] Economic Research Service, Farm income and wealth statistics, US Department of Agriculture (2024).
URL `https://www.ers.usda.gov/data-products/farm-income-and-wealth-statistics/`

[2] T. I. Zohdi, A machine-learning enabled digital-twin framework for next generation precision agriculture and forestry, Computer Methods in Applied Mechanics and Engineering 428 (2024) 117250. `doi:10.1016/j.cma.2024.117250`.

[3] E. Mengi, C. J. Becker, M. Sedky, S. Yu, T. I. Zohdi, A digital-twin and rapid optimization framework for optical design of indoor farming systems, Computational Mechanics 72 (2023) 953–970. `doi:10.1007/s00466-023-02421-9`.

[4] P. Goodrich, O. Betancourt, A. Arias, T. I. Zohdi, Placement and drone flight path mapping of agricultural soil sensors using machine learning, Computers and Electronics in Agriculture 198 (2022) 107591. doi:10.1016/j.compag.2022.107591.

[5] I. Tagkopoulos, S. F. Brown, X. Liu, Q. Zhao, T. I. Zohdi, J. M. Earles, N. Nitin, D. E. Runcie, D. G. Lemay, A. D. Smith, P. C. Ronald, H. Feng, G. D. Youtsey, Special report: AI institute for next generation food systems (AIFS), Computers and Electronics in Agriculture 196 (2022) 106819. doi:10.1016/j.compag.2022.106819.

[6] P.-F. Verhulst, Notice sur la loi que la population suit dans son accroissement, Correspondance mathématique et physique 10 (1838) 113–126. doi:10.1007/BF02309004.

[7] J. W. Jones, G. Hoogenboom, C. H. Porter, K. J. Boote, W. D. Batchelor, L. Hunt, P. W. Wilkens, U. Singh, A. J. Gijsman, J. T. Ritchie, The dssat cropping system model, European Journal of Agronomy 18 (3-4) (2003) 235–265. doi:10.1016/S1161-0301(02)00107-7.

[8] D. P. Holzworth, N. I. Huth, P. G. deVoil, E. J. Zurcher, N. I. Herrmann, G. McLean, K. Chenu, E. J. van Oosterom, V. Snow, C. Murphy, et al., Apsim–evolution towards a new generation of agricultural systems simulation, Environmental Modelling & Software 62 (2014) 327–350. doi:10.1016/j.envsoft.2014.07.009.

[9] C. Van Diepen, J. Wolf, H. Van Keulen, C. Rappoldt, Wofost: a simulation model of crop production, Soil Use and Management 5 (1) (1989) 16–24. doi:10.1111/j.1475-2743.1989.tb00755.x.

[10] R. Gebbers, V. I. Adamchuk, Precision agriculture and food security, Science 327 (5967) (2010) 828–831. doi:10.1126/science.1183899.

[11] A. Singh, An overview of the optimization modelling applications, Journal of Hydrology 466–467 (2012) 167–182. doi:10.1016/j.jhydrol.2012.08.004.

[12] J. E. Epperson, J. E. Hook, Y. R. Mustafa, Dynamic programming for improving irrigation scheduling strategies of maize, Agricultural Systems 42 (1) (1993) 85–101, applications of

Dynamic Optimization Techniques to Agricultural Problems. doi:https://doi.org/10.1016/0308-521X(93)90070-I.
URL https://www.sciencedirect.com/science/article/pii/0308521X9390070I

[13] W. Ding, C. Lin, Application of genetic algorithms to agriculture: a review, Computers and Electronics in Agriculture 175 (2020) 105524. doi:10.1016/j.compag.2020.105524.

[14] D. E. Goldberg, Genetic Algorithms in Search, Optimization, and Machine Learning, Addison-Wesley, Reading, MA, 1989.

[15] R. Wardlaw, K. Bhaktikul, Application of genetic algorithms for irrigation water scheduling, Irrigation and Drainage 53 (4) (2004) 397–414. doi:10.1002/ird.121.

[16] Z. Yu, W. Fu, Optimization of nitrogen fertilization strategies for drip irrigation of cotton in large fields by dssat combined with a genetic algorithm, Applied Sciences 15 (7) (2025) 3580.

[17] M. Sengupta, Y. Xie, A. Lopez, A. Habte, G. Maclaurin, J. Shelby, The national solar radiation data base (nsrdb), Renewable and Sustainable Energy Reviews 89 (2018) 51–60. doi:10.1016/j.rser.2018.03.003.

[18] National Oceanic and Atmospheric Administration, Climate data online (2024).
URL https://www.ncdc.noaa.gov/cdo-web/

[19] J. E. Sawyer, E. D. Nafziger, G. W. Randall, L. G. Bundy, G. W. Rehm, B. C. Joern, Nitrogen management for corn production, Iowa State University Extension Publication PM 1714 (2006).

[20] J. O. Payero, D. D. Tarkalson, S. Irmak, D. R. Davison, J. L. Petersen, Effect of irrigation amounts applied with subsurface drip irrigation on corn evapotranspiration, yield, water use efficiency, and dry matter production in a semiarid climate, Agricultural Water Management 95 (8) (2008) 895–908. doi:10.1016/j.agwat.2008.02.015.

[21] B. Sánchez, A. Rasmussen, J. R. Porter, Temperatures and the growth and development of maize and rice: a review, Global Change Biology 20 (2) (2014) 408–417. doi:10.1111/gcb.12389.

[22] R. C. Lewontin, D. Cohen, On population growth in a randomly varying environment, Proceedings of the National Academy of Sciences 62 (4) (1969) 1056–1060. doi:10.1073/pnas.62.4.1056.

[23] L. J. Abendroth, R. W. Elmore, M. J. Boyer, S. K. Marlay, In corn growth and development, Iowa State University Extension Publication PMR 1009 (2011).

[24] US Department of Agriculture, 2023 acreage data as of august 9, 2023 (2023).

[25] J. Sawyer, E. Nafziger, G. Randall, L. Bundy, G. Rehm, B. Joern, Concepts and rational for regional nitrogen rate guidelines for corn, University Extension Iowa State University Ames (2006).

[26] F. Schierbaum, Book reviews: Corn: Chemistry and technology, 2nd edition. by pamela j. white and lawrence a. johnson (editors), Starch-starke - STARCH 56 (2004) 263–264. doi:10.1002/star.200490027.

[27] W. L. Kranz, S. Irmak, S. J. van Donk, C. D. Yonts, D. L. Martin, Irrigation management for corn, Tech. Rep. G1850, University of Nebraska–Lincoln Extension (2008).
URL https://extensionpubs.unl.edu/publication/g1850/

[28] B. Davies, J. A. Coulter, P. H. Pagliari, Timing and rate of nitrogen fertilization influence maize yield and nitrogen use efficiency, PLOS ONE 15 (5) (2020) e0233674. doi:10.1371/journal.pone.0233674.

[29] F. J. Richards, A flexible growth function for empirical use, Journal of Experimental Botany 10 (2) (1959) 290–301. doi:10.1093/jxb/10.2.290.

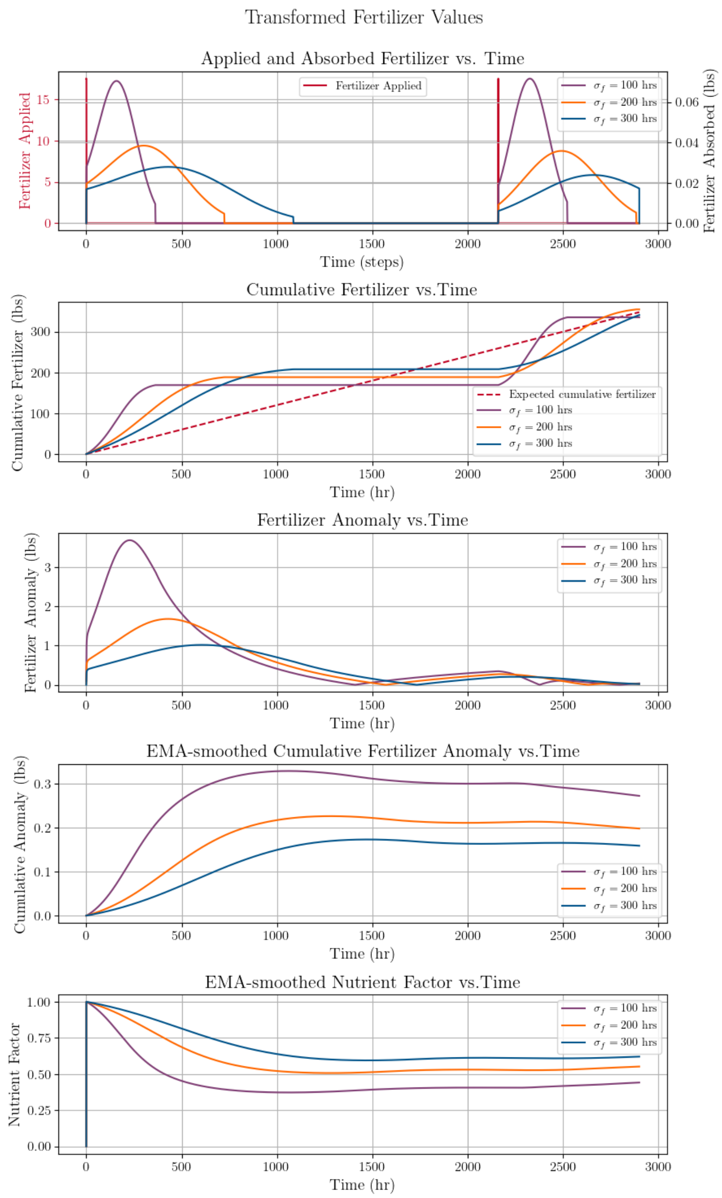

Figure 1: Illustration of the metabolic transformation pipeline. Panel 1: Gaussian FIR kernels with different temporal spreads σ demonstrate how water ($\sigma_w = 30$ hr) is absorbed more rapidly than fertilizer ($\sigma_f = 300$ hr). Panel 4: EMA filters with different memory parameters β show how cumulative divergence tracking responds to sustained anomalies, with larger β providing longer memory of past stress events.

Algorithm 1 Genetic Algorithm for Input Optimization

Input: Population size M, parents P, children C, generations G, bounds $[\mathbf{u}_{\min}, \mathbf{u}_{\max}]$
Output: Best solution $\mathbf{u}^*$

Initialize population $\{\mathbf{u}^{(1)}, \ldots, \mathbf{u}^{(M)}\}$ uniformly in bounds
Evaluate $\mathrm{Cost}(\mathbf{u}^{(i)})$ for all i via full-season simulation
Sort population by cost (ascending)
stagnation $\leftarrow 0$

for $g = 1$ to G **do**
    Selection: Keep top P members as parents

    Crossover: Generate C children
    for $j = 1$ to C **do**
        Select parents $\mathbf{u}^{(a)}$, $\mathbf{u}^{(b)}$ randomly from top P
        if stagnation < 10 **then**
            $\phi \sim \mathrm{Uniform}(0, 1)$
        else
            $\phi \sim \mathrm{Uniform}(-1, 2)$ ▷ Aggressive exploration
        end if
        $\mathbf{u}^{(\text{child})} \leftarrow \phi \cdot \mathbf{u}^{(a)} + (1 - \phi) \cdot \mathbf{u}^{(b)}$
        Clip to bounds
    end for

    Fill remaining: Generate $M - P - C$ random members
    Evaluate costs for new members
    Sort population by cost

    Stagnation check:
    if $|\mathrm{Cost}^{(g)} - \mathrm{Cost}^{(g-1)}| < 0.01$ **then**
        stagnation $\leftarrow$ stagnation $+ 1$
    else
        stagnation $\leftarrow 0$
    end if
end for

return $\mathbf{u}^{(1)}$ (best member)

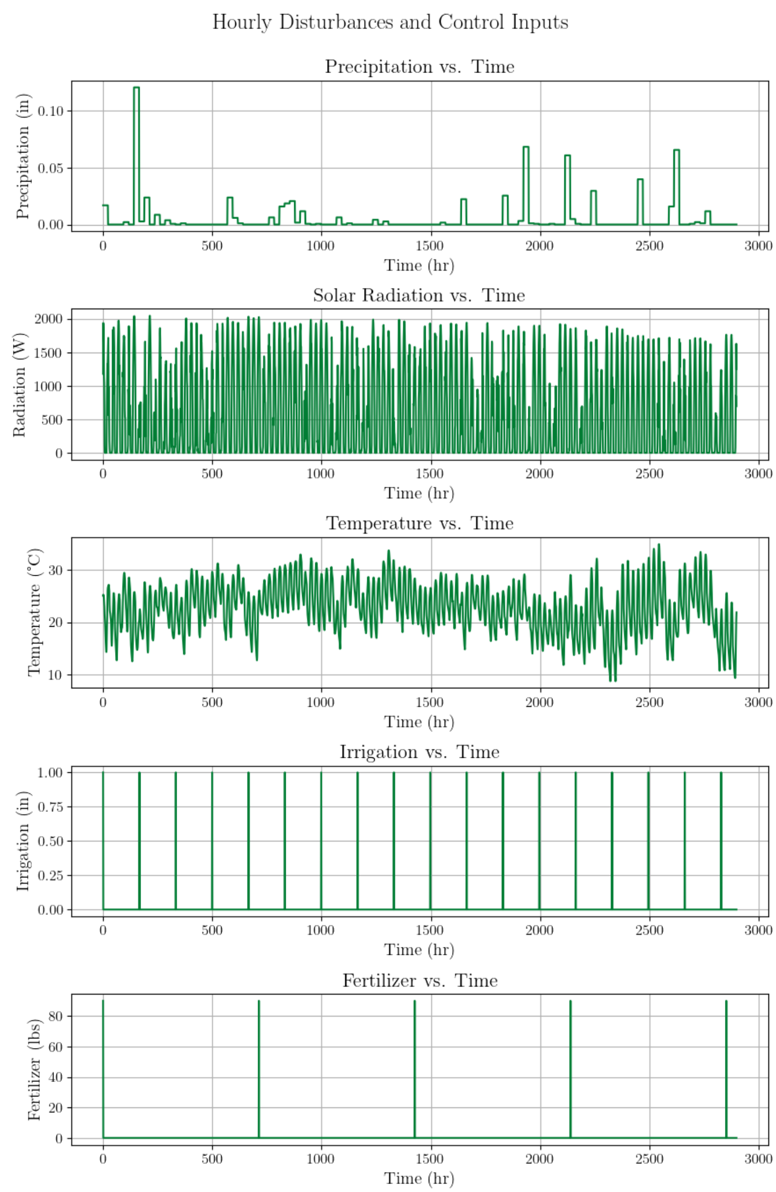

Figure 2: Environmental disturbances and control inputs for the baseline scenario. Top three panels show hourly precipitation (reduced to 50% of normal), solar radiation, and temperature from historical Iowa data. Bottom two panels show the farmer's irrigation (weekly, 1 inch) and fertilizer (monthly, 90 lbs) application strategy.

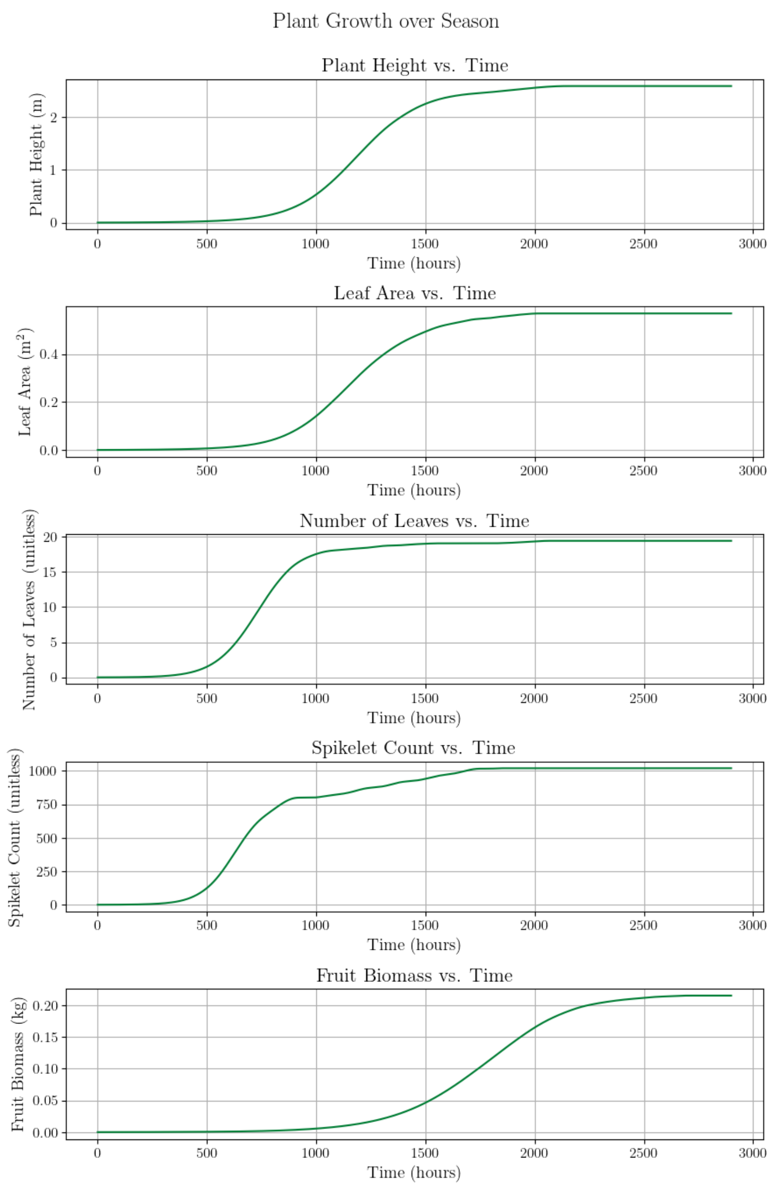

Figure 3: Plant state variable trajectories under the baseline scenario (farmer best practices during drought). All state variables reach suboptimal final values due to cumulative water stress. This strategy yields $859/acre in revenue.

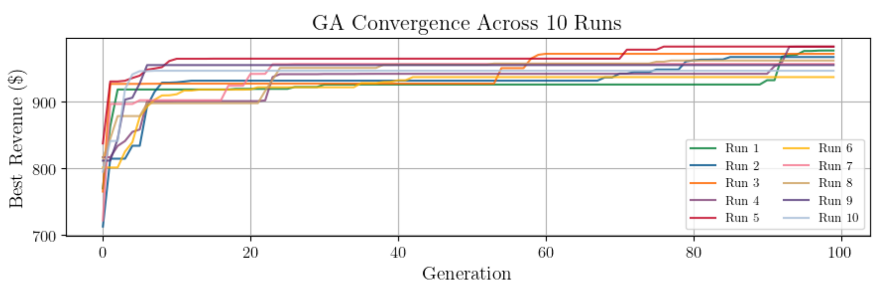

Figure 4: GA convergence across 10 independent runs. Each curve shows the best revenue at each generation. All runs exhibit rapid improvement in early generations followed by convergence to near-optimal solutions. The consistency across runs demonstrates algorithm robustness.

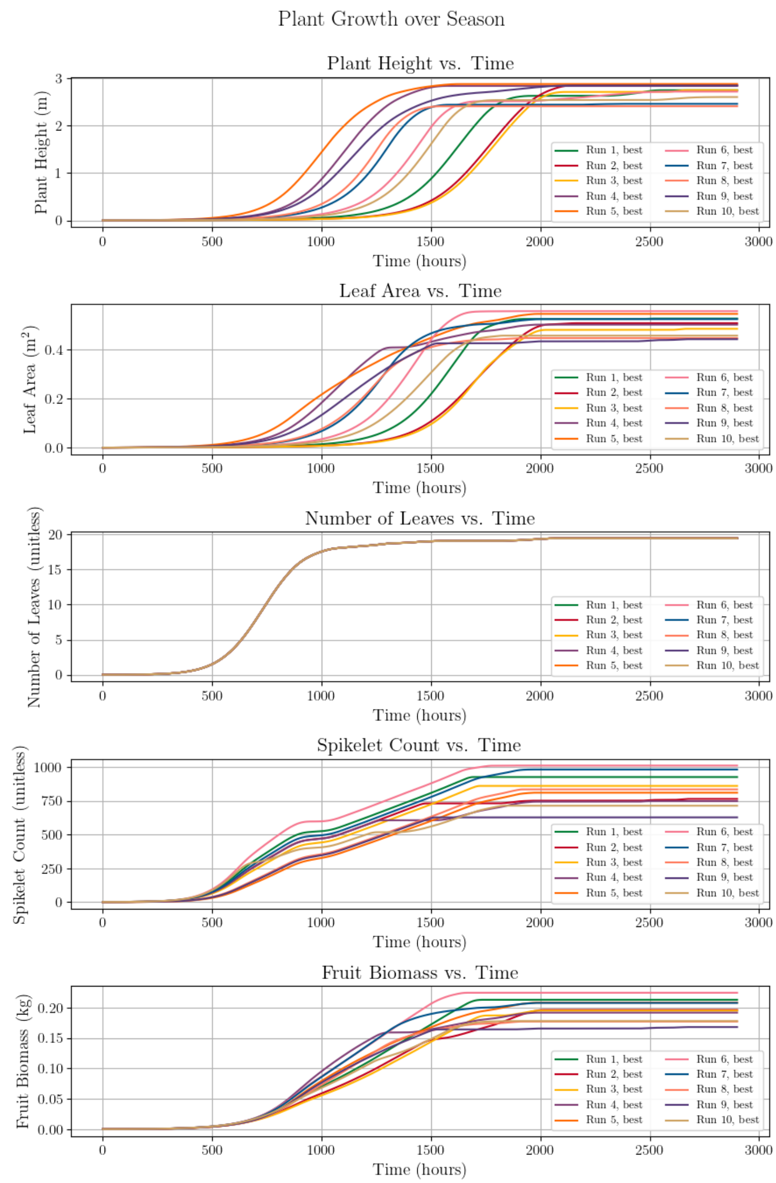

Figure 5: Plant state variable trajectories for the best member from each of the 10 independent GA runs. All optimized strategies achieve similar, near-optimal growth trajectories, and 9 of 10 runs substantially outperform the baseline farmer practices (Figure 3). The tight clustering of trajectories demonstrates that different GA runs converge to similar optimal strategies.

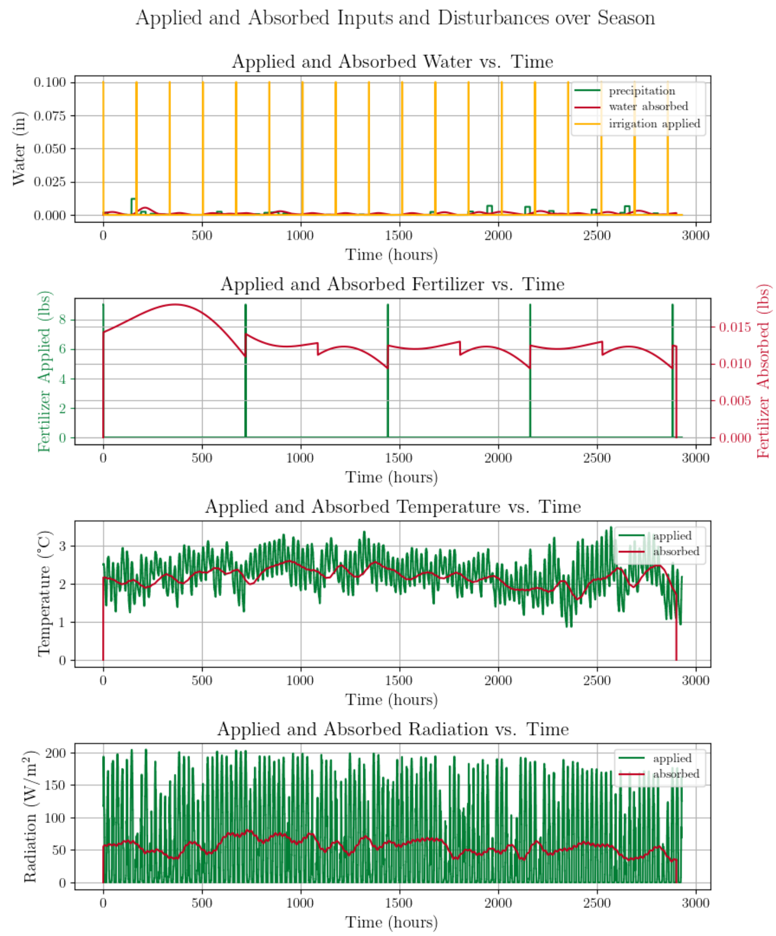

Figure 6: Applied versus absorbed nutrients under the baseline farmer strategy. The delayed absorption dynamics are evident in the lag between applied inputs and the smoothed absorbed signals. Water absorption ($\sigma_w = 30$ hr) responds more quickly than fertilizer absorption ($\sigma_f = 300$ hr).

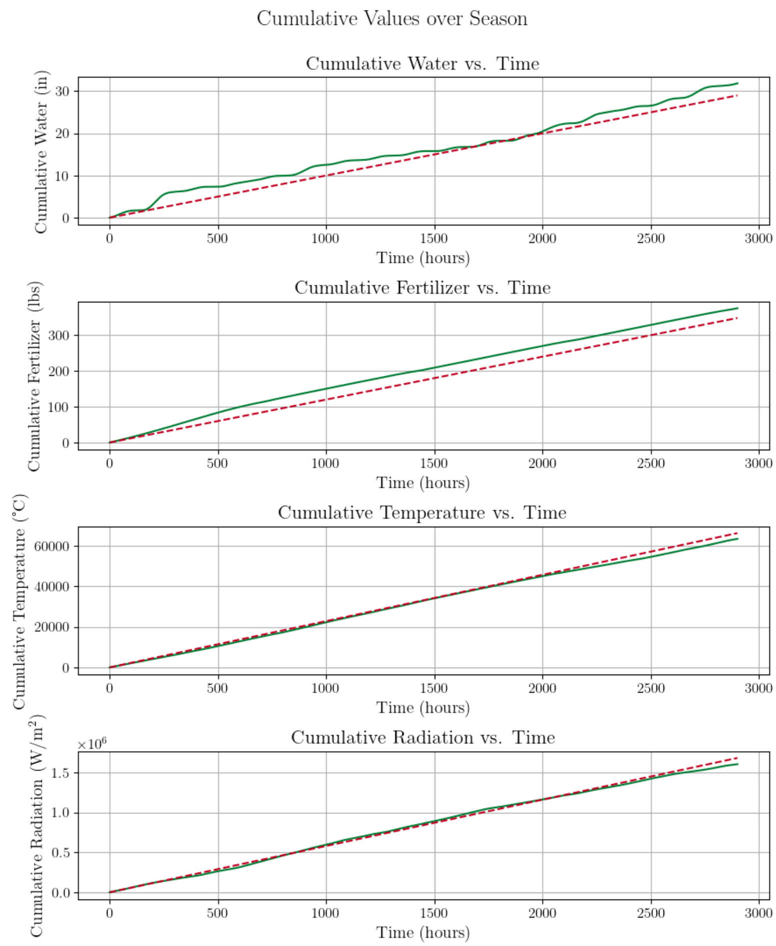

Figure 7: Cumulative absorbed nutrients (solid) versus expected levels (dashed red). The growing gap between actual and expected water absorption reflects the drought stress accumulating over the season. Fertilizer applications maintain closer alignment with expectations.

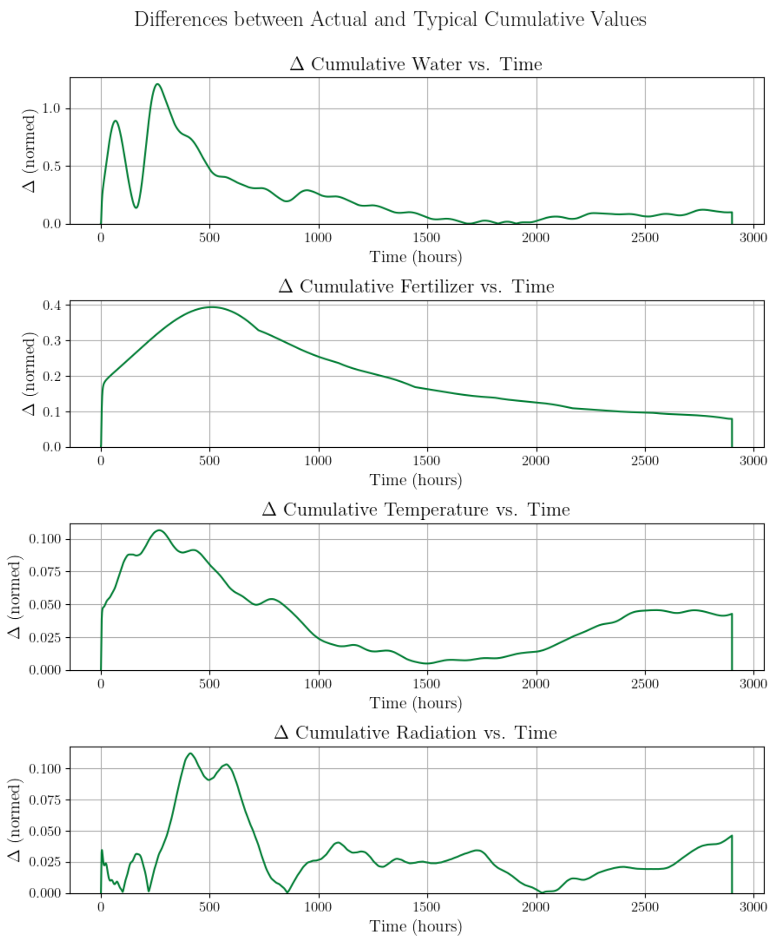

Figure 8: Instantaneous divergence from expected cumulative nutrient levels. Higher divergence indicates greater stress. The water divergence grows throughout the season due to cumulative drought effects.

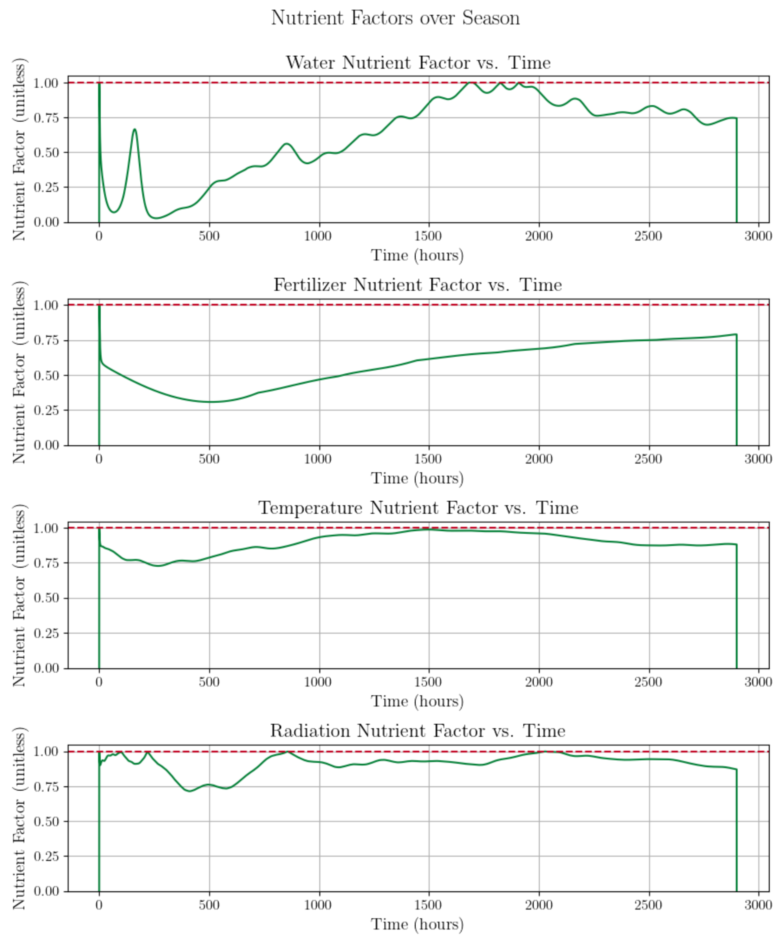

Figure 9: Nutrient factor evolution under the baseline scenario. The water factor ν_w declines due to cumulative drought stress, while fertilizer, temperature, and radiation factors remain closer to 1.0 (no stress). The declining ν_w reduces effective growth rates and carrying capacities throughout the season.

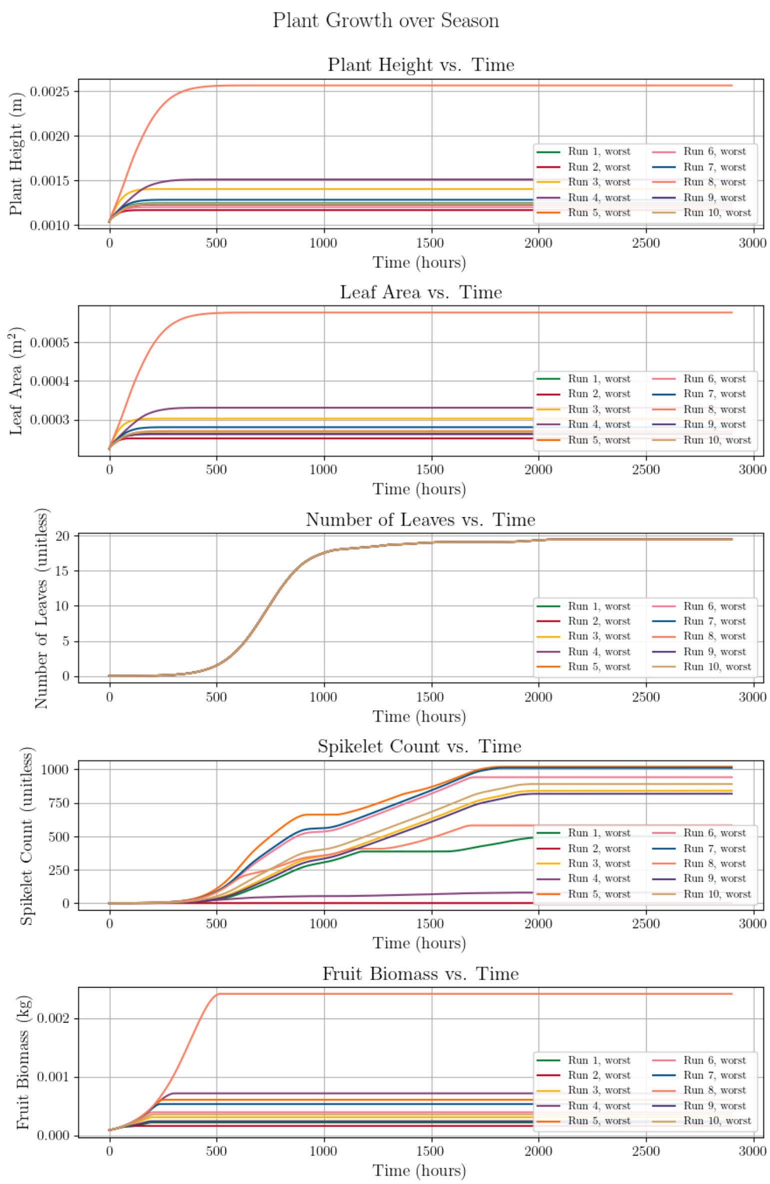

Figure 10: Plant state variable trajectories for the worst member from each GA run's final population. Even these suboptimal strategies outperform baseline farmer practices (compare to Figure 3), demonstrating that the GA successfully identifies the high-performing region of the strategy space and that random strategies are not competitive.